Human Molecular Genetics, 2000, Vol. 9, No. 17 **2491–2506**

ARTICLE

Expanded polyglutamines induce neurodegeneration and trans-neuronal alterations in cerebellum and retina of SCA7 transgenic mice

Gaël Yvert[1], Katrin S. Lindenberg[2,3], Serge Picaud[4], G. Bernhard Landwehrmeyer[2,3], José-Alain Sahel[4] and Jean-Louis Mandel[1,+]

[1]Institut de Génétique et de Biologie Moléculaire et Cellulaire, CNRS/INSERM/ULP, BP 163, 67404 Illkirch cedex, CU de Strasbourg, France, [2]Department of Neurology, Albert Ludwigs-University, 79106 Freiburg, Germany, [3]Department of Neurology, University of Ulm, 89075 Ulm, Germany and [4]Laboratoire de physiopathologie de la rétine, INSERM EMI-99–18, Université Louis Pasteur, BP 426, 67091 Strasbourg cedex, France

Received 10 July 2000; Revised and Accepted 23 August 2000

Among the eight progressive neurodegenerative diseases caused by polyglutamine expansions, spinocerebellar ataxia type 7 (SCA7) is the only one to display degeneration in both brain and retina. We show here that mice overexpressing full-length mutant ataxin-7[Q90] either in Purkinje cells or in rod photoreceptors have deficiencies in motor coordination and vision, respectively. In both models, although with different time courses, an N-terminal fragment of mutant ataxin-7 accumulates into ubiquitinated nuclear inclusions that recruit a distinct set of chaperone/proteasome subunits. A severe degeneration is caused by overexpression of ataxin-7[Q90] in rods, whereas a similar overexpression of normal ataxin-7[Q10] has no obvious effect. The degenerative process is not limited to photoreceptors, showing secondary alterations of post-synaptic neurons. These findings suggest that proteolytic cleavage of mutant ataxin-7 and trans-neuronal responses are implicated in the pathogenesis of SCA7.

INTRODUCTION

Dysfunction, degeneration and loss of distinct neuronal populations in cerebellum and brainstem are the hallmarks of autosomal dominant ataxias including spinocerebellar ataxia type 7 (SCA7). The mutation responsible for SCA7 is an expansion of a trinucleotide CAG repeat coding for a polyglutamine stretch in the N-terminal domain of a protein (ataxin-7) of unknown function (1). Therefore, SCA7 belongs to a family of neurodegenerative disorders including SCA1–3, SCA6 and spinal bulbar muscular atrophy (SBMA or Kennedy's disease), dentatorubral-pallidoluysian atrophy (DRPLA) and Huntington's disease (HD), all caused by polyglutamine-coding CAG expansions in the otherwise unrelated target genes (2). SCA7 differs from the other polyglutamine disorders in that the pathological phenotype includes a mottled appearance of the macula with pigment epithelium alterations and photoreceptor atrophy leading to visual loss. Pathologically, the retina of patients with SCA7 is characterized by a loss of rods, cones and ganglion cells and migration of pigmented cells into the retinal layers (3).

Studies in the last 3 years have shown that polyglutamine disorders are associated with the formation of neuronal intranuclear ubiquitinated inclusions containing at least part of the mutant protein (2). Recently, two studies reported such inclusions in brain and retina of SCA7 patients (4,5). Although the presence of these inclusions is observed in the various diseases, several observations have led us to question their direct impact on neuronal toxicity. Inclusions have been observed in both vulnerable and relatively resistant populations of neurons in HD (6,7) and SCA7 (4) patients . Secondly, a similar strong neurological phenotype is observed in mice overexpressing forms of mutant ataxin-1 that either form nuclear inclusions or do not form such aggregates because of a supplementary mutation in its self-association domain (8). Thirdly, in the context of a ubiquitin ligase *Ube3A* null mutation, SCA1 transgenic mice develop fewer aggregates, but showed stronger and accelerated Purkinje cell pathology (9).

Ataxin-7 appears to be located in the nucleus of lymphoblastoid and transfected COS cells (10,11). In human neurons, however, ataxin-7 immunoreactivity is not exclusively localized in the nucleus: a recent study on human brain sections demonstrated both nuclear and cytoplasmic localizations (12). Several studies suggest that the nucleus is the prime target for polyglutamine-mediated pathogenesis. A mutation in a nuclear localization signal of ataxin-1 relocalizes it to the cytoplasm and mice overexpressing ataxin-1[Q82] with this mutation

+To whom correspondence should be addressed. Tel: + 33 3 88 65 34 12; Fax: + 33 3 88 65 34 42; Email: mandeljl@igbmc.u-strasbg.fr

show no pathological phenotype (8). Mutated huntingtin and atrophin-1 were shown to translocate from the cytoplasm to the nucleus in cell culture systems, mouse models (13–17) and patient material (6,16). However, the nucleus is probably not the only site of polyglutamine toxicity. HD patients also show abnormal cytoplasmic aggregates in neurons of affected brain regions (6,7).

To study the retinal degeneration caused by the SCA7 mutation, we have generated several lines of transgenic mice in which the rhodopsin promoter (18,19) drives the expression of the full-length human ataxin-7 with 90 or 10 glutamines (R7E and R7N, respectively) in rod photoreceptors. R7E but not R7N animals developed a progressive retinal degeneration accompanied by the formation of ataxin-7[Q90]-containing nuclear inclusions (NIs). NIs were not immunoreactive for the C-terminal epitope of ataxin-7 (distal to the polyglutamine tract), suggesting that a proteolytic processing of mutant ataxin-7 may be part of the SCA7 pathology. Effects of mutant ataxin-7 were not limited to the cell type expressing the transgene: we observed morphological anomalies in post-synaptic interneurons. The features observed in retina could be specific to photoreceptors and may not occur in other neurons affected in SCA7. Therefore, we also investigated the toxicity of ataxin-7[Q90] in Purkinje neurons by generating transgenic animals (P7E) where expression is driven by the Purkinje cell specific pcp-2 promoter (20,21). The line with the highest expression level showed locomotion deficiencies and pathological features similar to those of retinas in R7E.

This work provides an example of anomalies occurring in cell types that do not express the polyglutamine mutation, but are postsynaptic to targeted neurons. Due to the accessibility of the retina and its *in vivo* functional monitoring by electroretinography, SCA7 mice offer new opportunities for therapeutic research on triplet repeat disorders.

RESULTS

Generation of transgenic lines expressing full-length human ataxin-7

We have generated transgenic mice overexpressing full-length human ataxin-7 using four different constructs (Fig. 1A). The P7E and P7N constructs are transcriptionally regulated by the *pcp-2* promoter which drives expression specifically in Purkinje cells and was previously used to overexpress mutant ataxin-1 in SCA1 mouse models (8,21). The R7E and R7N constructs are under the control of a 2 kb regulatory region of the human rhodopsin gene containing the RER enhancer element (22). All constructs harbor the full-length human SCA7 open reading frame (1) with 720 bp of SCA7 3′-UTR, followed by an intron and a polyadenylation site. P7E and R7E carry a $(CAG)_{90}$ repeat expansion, whereas the P7N and R7N controls have a $(CAG)_{10}$ repeat, corresponding to the most frequent allele in the normal population. Lines were then amplified on the C57BL/6 background to avoid the presence of the *rd* (retinal degeneration) mutation (23). The number of founders obtained after the injection of each construct is indicated in Table 1. Their progeny were genotyped by Southern blot for determination of the number of integration sites and the approximate transgene copy number per site. Crosses were then designed to obtain lines with single integration sites. The resulting lines are listed in Table 1.

Table 1. Transgenic SCA7 lines

Transgene	No. of founders	Lines	Copy number[a]	Protein expression[b]
P7E	5[c]	B	10–50	+++
		C	>100	+
		E	5–10	+
P7N	4	A	50–100	–
		B	>100	–
		C	10–50	–
		D	10–50	–
R7E	5[d]	A	5–10	++++
		B	>100	++
		C	1	+++
		D	10–50	–
		F	1–5	++++
R7N	3	A	1–5	++
		B	10–50	+
		C	50–100	++++

[a]Approximate copy numbers were estimated from Southern blot of tail DNA digested by restriction enzymes that cut once in the transgenes.
[b]Expression was estimated by immunofluorescence using the 1261, 1262 and 1C1 antibodies. R7E and R7N constructs were not expressed in all rod cells and comparison between lines reflects the proportion of expressing cells. In contrast, the P7E construct was expressed in all Purkinje cells although at different levels depending on the line.
[c]Two P7E founders did not transmit the transgene.
[d]One R7E founder had two integration sites leading to lines R7EA and R7EC and one founder did not tansmit the transgene.

Expression in each line was assessed by immunofluorescence using three different SCA7 antibodies: 1261, 1262 and 1C1 (12). All three antibodies gave no signal on non-transgenic sections, suggesting a low expression of endogenous ataxin-7 (shown for 1261 in Fig. 1B). In all cases, expression appeared strictly limited to the targeted cell type (Fig. 1B and C) and no correlation was seen between copy numbers and expression levels. The P7E lines showed expression in all Purkinje cells and differed by the level of immunoreactivity per cell. We focused on the P7E.B line which showed the highest expression level (Table 1). We were unable to detect normal ataxin-7 in the P7N lines with any of the antibodies, therefore these lines were not used further. Both R7E and R7N lines differed in the number of expressing rod cells, with a strong signal in all positive cells. We further characterized the R7E.A, R7E.F and R7N.C lines because of their higher percentage of expressing cells.

We also studied expression of ataxin-7[Q90] by western blot (Fig. 1D). Due to its higher sensitivity compared with our SCA7 antibodies, we used the 1C2 antibody which detects expanded polyglutamines (10). Mutant ataxin-7 is visible in retinal extracts of R7E animals at the expected 150 kDa size, when compared with a lymphoblastoid cell extract from an SCA7 patient. Western blotting did not detect mutant ataxin-7

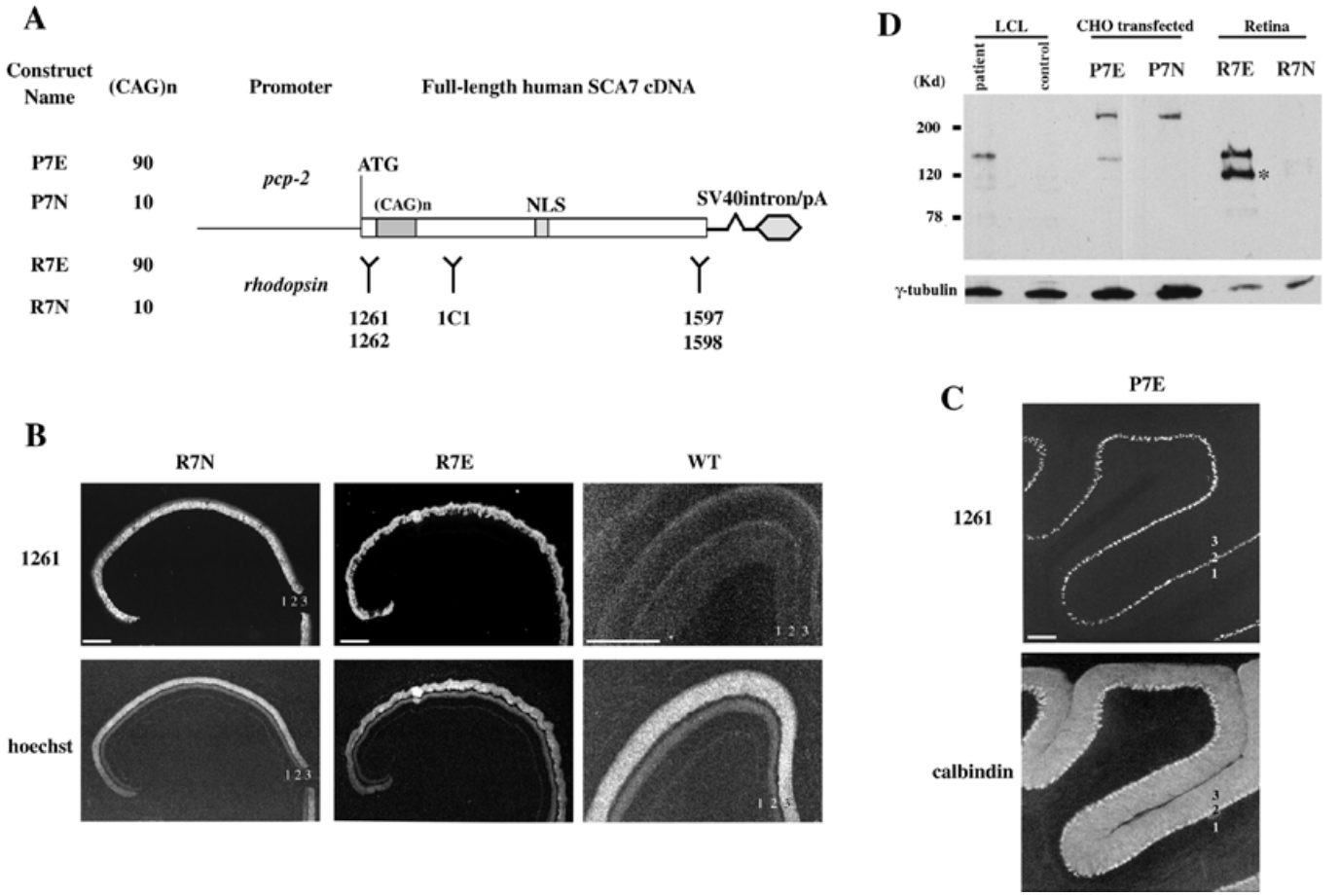

Figure 1. Ataxin-7 expression in transgenic mice. (**A**) Schematic view of transgene constructs and epitopes. (**B**) Immunofluorescence of retinas from 2-month-old wild-type, R7E (line A) and R7N (line C) transgenic animals using the 1261 antibody. Both R7E and R7N animals show a strong ataxin-7 immunoreactivity exclusively in photoreceptors. No staining is observed in non-transgenic animals. 1, ganglion cell layer; 2, inner nuclear layer; 3, outer nuclear layer; WT, wild-type. Bars, 250 µm. (**C**) Immunofluorescence of cerebellum from a 7-month-old P7E transgenic animal (line B). Ataxin-7[Q90] (top) is found in all Purkinje cell nuclei and is restricted to the Purkinje cell layer. For comparison, the calbindin staining (bottom) shows both somata and dendritic arbours of Purkinje cells. 1, granular cell layer; 2, Purkinje cell layer; 3, molecular cell layer. Bars, 250 µm. (**D**) Western blot analysis of expression using the 1C2 antibody (10). Mutant ataxin-7 is detected at 150 kDa in a patient's cell line extract, in retinas from 21-day-old R7E animals and in CHO cells transfected with the P7E construct. CHO extracts show a cross-reactive band of >200 kDa, also present in non-transfected cell extracts (data not shown). Note the cleaved product at 120 kDa in R7E extracts (*).

from P7E cerebellar extracts, not even as insoluble material stacked in the top of the gel (data not shown). We thus confirmed the P7E construct integrity by transfection in Chinese hamster ovary (CHO) cells which are known to express *pcp-2*-driven constructs (24). These transfected cell extracts contained the expected 150 kDa product.

Mutant ataxin-7 progressively forms nuclear inclusions in transgenic mice

We investigated the distribution of ataxin-7 by immunohistochemistry at different ages (Fig. 2). We found that ataxin-7[Q90] progressively forms inclusions, whereas ataxin-7[Q10] does not. In Purkinje cells of 1-month-old P7E animals, ataxin-7 immunoreactivity was confined to the nucleus (Fig. 2A). The nucleus appeared homogenously labeled with dot-like focal accentuations of immunoreactivity preferentially in a perinucleolar localization; immunoreactivity in the nucleolus was low. At 4 months, nuclear ataxin-7 immunoreactivity in most Purkinje cells appeared more intense; in some Purkinje cell nuclei, in particular the more rostral lobes of the cerebellum (lobes 1–8), multiple minute ataxin-7-positive inclusions were detectable. At 8 months, many cells had developed multiple ataxin-7-immunoreactive NIs in addition to an intense general nuclear staining. At 16 months, most Purkinje cells contained a single large NI, often in the vicinity of the nucleolus. These large inclusions displayed an intense ataxin-7 immunoreactivity at the expense of the overall nuclear ataxin-7 signal which appeared to decrease in intensity. Electron microscopic examination confirmed that NIs were located close to the nucleolus. The time-course for the formation of NIs was not uniform throughout the cerebellum: Purkinje cells located in cerebellar lobules 9 (uvula) and 10 (nodule) developed nuclear enrichment of ataxin-7 immunoreactivity and NIs later than Purkinje cells in lobules 1–8. These regional differences may reflect a positional effect of the transgene integration site, be a property of the pcp-2 promoter, or may indicate regional differences in the metabolism of ataxin-7.

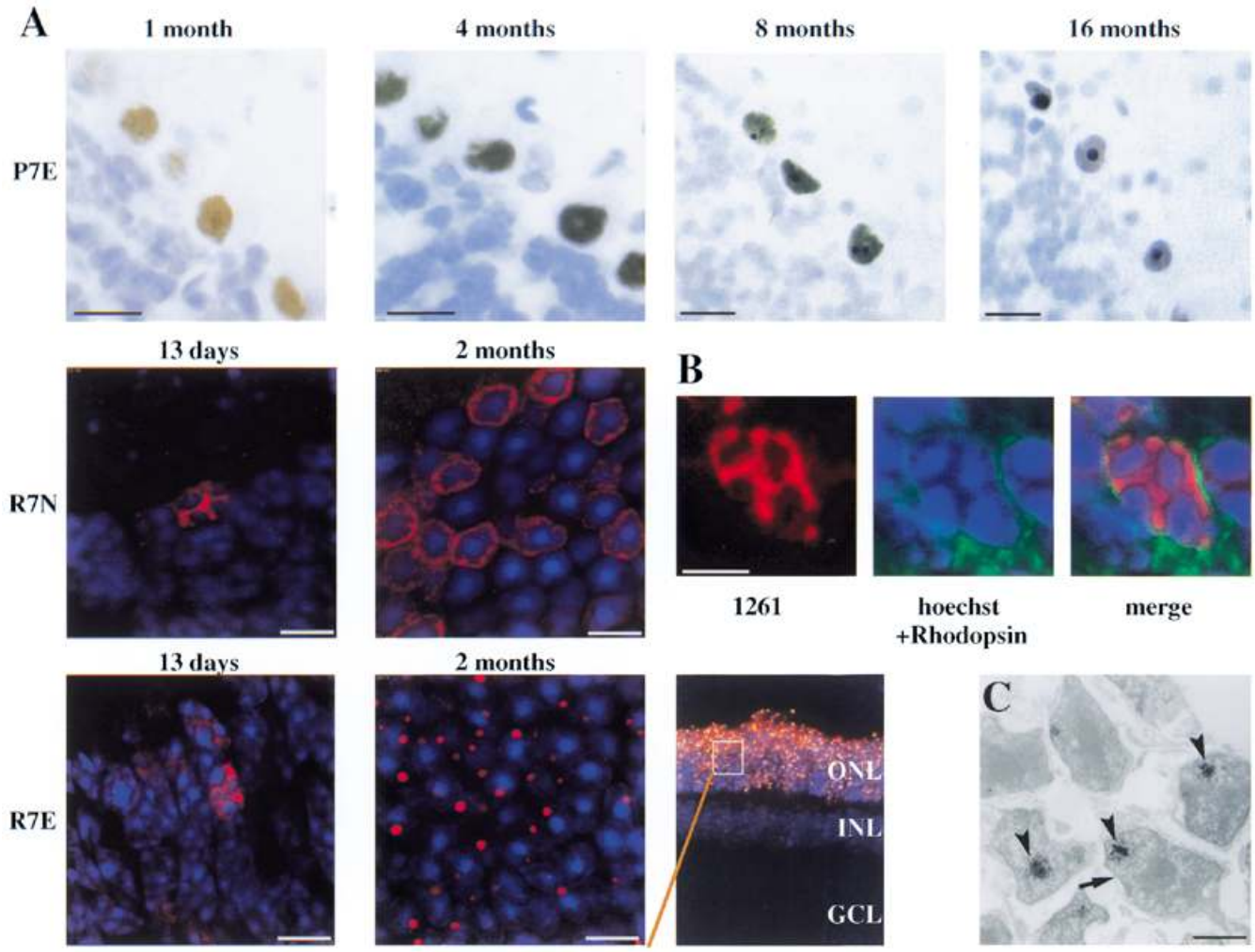

Figure 2. Cellular localization of human ataxin-7 in transgenic mice. (**A**) Time course of aggregation of mutant ataxin-7. Cerebellar (upper panels) paraffin sections from P7E transgenic animals (line B) of different ages were stained with the 1261 antibody using the immunoperoxidase method and counterstained with hematoxylin. At all stages the protein is nuclear and accumulates progressively. Retinal frozen sections (lower panels) from R7E (line A) and -N (line C) transgenic animals of indicated ages were stained with 1261 (red) and counterstained with Hoechst (blue). At 13 days, both normal and mutant ataxin-7 have an 'alveolar' distribution. Within 2 months, mutant ataxin-7 progressively aggregates in inclusions (as also shown at a lower magnification), whereas the normal protein distributes around the nucleus. At this age, normal ataxin-7 also localizes in the inner segments (data not shown). Black bar, 20 µm; white bar, 8 µm. (**B**) Ataxin-7 is nuclear in photoreceptors at 13 days. Confocal immunofluorescence using the 1261 (red) and Rho4D2 (green) antibodies, and counterstained with Hoechst (blue). The 'alveolar' pattern of ataxin-7 immunoreactivity at 13 days corresponds to a nuclear localization. Bar, 4 µm. (**C**) Immuno-electron microscopy of R7E rods. Retina from a 2.5-month-old R7E animal was stained using the 1261 antibody and DAB immunoperoxidase labeling. All immunoreactive inclusions are nuclear. Arrowheads, nuclear membrane. Bar, 4 µm.

Inclusions in R7E photoreceptors formed much faster than in P7E Purkinje cells. At 13 days, in retina of both R7N and R7E animals, ataxin-7 immunoreactivity was found in an 'alveolar' nuclear distribution pattern. Double labeling with the anti-ataxin-7 antibody 1261 and an anti-rhodopsin antibody using confocal laser microscopy and counterstaining with the Hoechst dye showed that the 'alveolar' immunoreactivity represented nuclear signals of individual cells (Fig. 2B). At later ages, ataxin-7 immunoreactivity was progressively concentrated in large inclusions, whereas nuclear signals outside the inclusion decreased or faded to background intensity. By fluorescent immunohistochemistry the inclusions appeared to flank the signals obtained by counterstaining with the Hoechst dye, raising the possibility of a perinuclear localization (Fig. 2A). Electron microscopy of a 2.5-month-old R7E retina stained with 1261 demonstrated that all inclusions were indeed intranuclear (Fig. 2C). Intriguingly, in the retina of R7N animals (2 months old) ataxin-7 immunoreactivity was found in both the extranuclear perisomal area and the inner segments, suggesting a cytoplasmic localization of normal ataxin-7 in photoreceptors at adult age (Fig. 2A). Similarly, at 1 month old, ataxin-7 immunoreactivity in R7E animals also localized

in the cytoplasm. In addition, in the inner segments of some photoreceptors we observed dense accumulation of ataxin-7 immunoreactivity suggesting the presence of cytoplasmic aggregates of ataxin-7[Q90] (data not shown). After 2 months, however, this cytoplasmic immunoreactivity was only found in very few cells of R7E retinal sections. An example of such a cell is shown in Figure 3j. The non-nuclear aggregates were no longer detectable at later ages.

Mutant ataxin-7 is abnormally processed: accumulation of N-terminal fragments and loss of C-terminal immunoreactivities

In order to explore whether the full-length ataxin-7 protein is present in NIs, we generated two polyclonal antibodies (dubbed 1597 and 1598) directed against the last 20 residues of the protein. Two earlier studies were in contradiction about the amino acid sequence of the C-terminal end of ataxin-7 (1,25). This ambiguity was recently resolved by the characterization of the genomic organization of the *SCA7* human gene (26), confirming that the cDNA, antigens and antibodies used in our study correspond to the right sequence. The specificity of the 1597 and 1598 C-terminal antibodies was assessed by western blot and immunofluorescence, 1598 giving the weakest background with no signal on non-transgenic retinal sections (data not shown). Immunofluorescence using both 1597 and 1598 on R7N transgenic retinas resulted in a signal similar to that of the 1261 N-terminal antibody (Fig. 3n).

For a direct comparison of the fate of the N- and C-terminal parts of ataxin-7, we performed double immunofluorescence using the 1C1 monoclonal (12) and 1598 polyclonal antibodies on retinal sections (Fig. 3). Incubation with both antibodies resulted in a similar signal in R7N transgenic retinas of different ages. In contrast, a marked difference of immunoreactivity appeared progressively in R7E retinas. At 13 days of age, R7E photoreceptors showed mainly an alveolar nuclear staining (identical to the pattern shown in Fig. 2B) with both 1C1 and 1598. At 20 days, staining with 1C1 resulted in both a uniformly distributed nuclear signal and focal accumulation of ataxin-7 immunoreactivity confirming the 1261 staining, whereas 1598 exclusively showed a uniform nuclear staining pattern. This difference was even more pronounced at 27 days. At 2 months of age, only a very few cells (<10 in the entire section) had a diffuse signal (cytoplasmic at this age as mentioned) and apart from these rare cells, no C-terminal immunoreactivity remained.

The lack of staining of the inclusions by 1598 (and by 1597; data not shown) is unlikely to result from a lower sensitivity of the antibody since it detected the homogenously distributed ataxin-7. Although we cannot exclude the possibility that the corresponding C-terminal epitopes of ataxin-7 were hidden within the inclusions and not accessible for detection, one more likely possibility is that ataxin-7[Q90] was cleaved and only an N-terminal product was present in the aggregates. The cleaved product observed on the western blot of R7E extracts at 21 days is consistent with such a proteolytic processing (Fig. 1D).

The apparent loss of 1598 immunoreactivity at 2 months suggests either that R7E photoreceptors did not express the transgene as well at this age as at 13 days, or that they developed a quicker turn-over of the C-terminal of ataxin-7[Q90]. In both cases, this response was correlated to the presence of the expansion mutation since the detection of ataxin-7[Q10] remained stable in R7N retinas (Fig. 3m–o).

In Purkinje cells of P7E animals, NIs were also not stained with the 1597 and 1598 antibodies (data not shown). The processing of mutant ataxin-7 is therefore common to both targeted cell types.

Table 2. Immunoreactivities of SCA7 nuclear inclusions

		Immunoreactivity of SCA7 inclusions in Purkinje cells and rods
Ubiquitin		+++
11S regulator units	α	–
	β	+
19S cap units	S4 (mts-2)	+++
	S5a	+
	S6b (TBP7)	–
	S7 (mss-1)	++
	S10b (p42)	–
20S core units	α3	+++
	α1, 2, 3, 5, 6 and 7	+++
	β2	+++
	β3	+
Chaperones	HDJ-2	+++
	HDJ-1	–

+++, almost all inclusions; ++, some inclusions; +, <10% inclusions; –, no inclusion.
This pattern of immunoreactivity was observed in R7E photoreceptors at 1, 2.7 and 7 months of age. At 7 months, the immunoreactivities of photoreceptors are stronger than at younger ages. The same pattern was observed in inclusions of P7E Purkinje cells at 8, 16 and 19 months.

Ubiquitin and a distinct set of chaperone and proteasome subunits is recruited into NIs

Induction of chaperones and protein degradation by the ubiquitin/proteasome pathway may be involved in the cellular response to the deposits of polyglutamine-expanded proteins (27). To investigate whether NIs in our animal models also contained protein actors of such a response, we tested a panel of antibodies recognizing chaperones and a set of distinct proteasomal subunits (Table 2). Using antibodies against Hsp40 chaperones, we found a high percentage of NIs labeled with HDJ-2 but not HDJ-1 (Fig. 4C and D). Almost all; NIs were found to be immunoreactive to ubiquitin antibodies (Fig. 4A and B). Poly-ubiquitination destines proteins for degradation through the proteasome pathway. Interestingly, a subset of, but not all, NIs were immunoreactive to an antibody recognizing the proteasomal subunit 5a, the putative recognition site of poly-ubiquitinated proteins. Almost all NIs were immunoreactive to a set of ATPase activity containing 19S subunits (Fig. 4E). Many, but not all, NIs displayed immunoreactivity to subunits of the proteolytic core of the 20S complex, suggesting that NIs are not all associated with all components

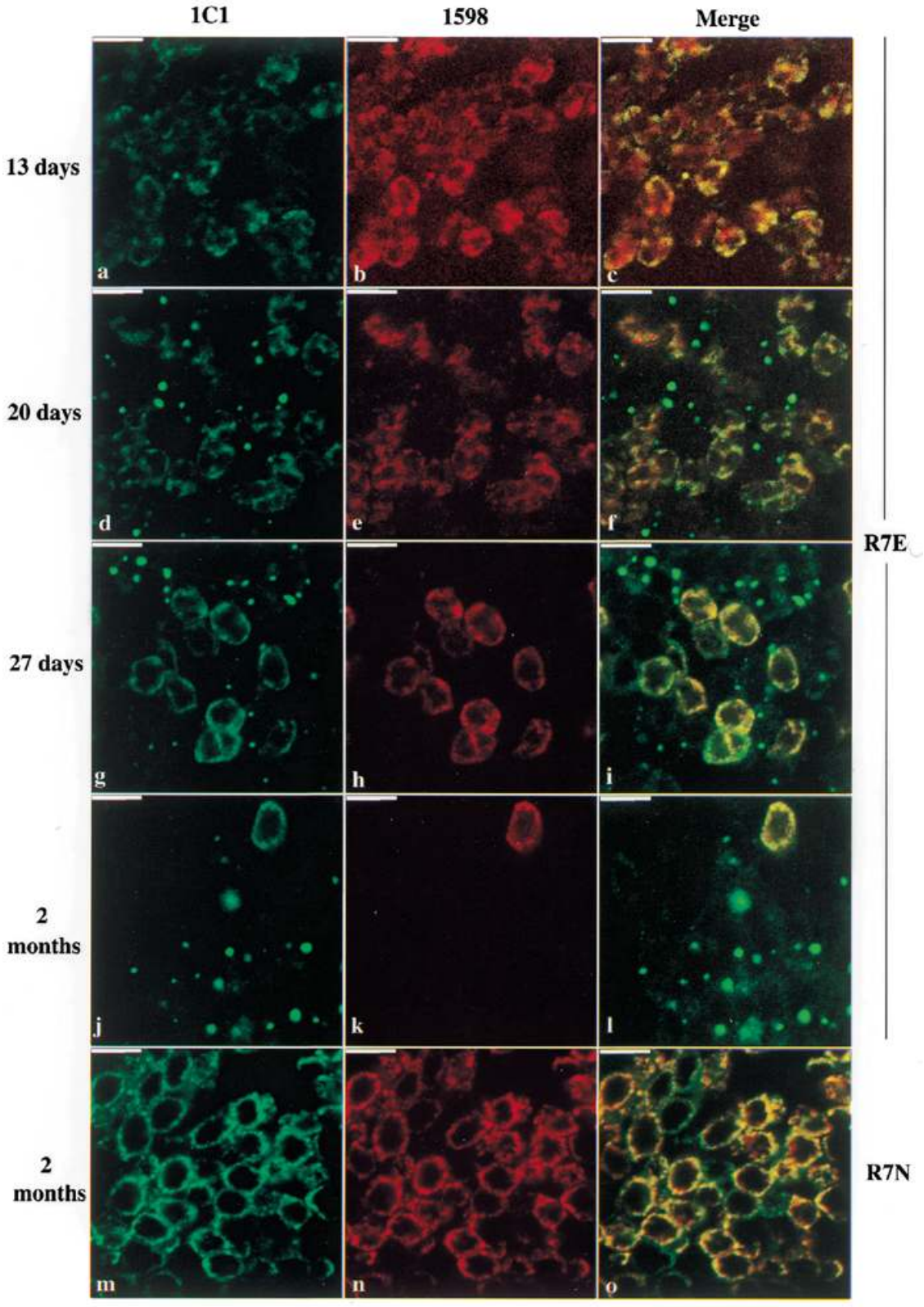

Figure 3. Mutated ataxin-7 is abnormally processed in transgenic mice. Immunofluorescence confocal microscopy on retinal sections of R7E (line A) (**a–l**) and R7N (line C) (**m–o**) animals double stained with the 1C1 (green) and 1598 (red) antibodies (yellow: merged signals). Animals were sacrificed at the ages indicated. NIs are immunoreactive for 1C1 but not for 1598. At 2 months old, only a couple of cells remained immunoreactive for 1598 in the entire R7E section (j–l). Both normal and mutant ataxin-7 relocalize to the cytoplasm at ~27 days (g–i and m–o). The 'alveolar' pattern at 13 days is the same as that revealed by 1261 in Figure 2. Bar, 8 μm.

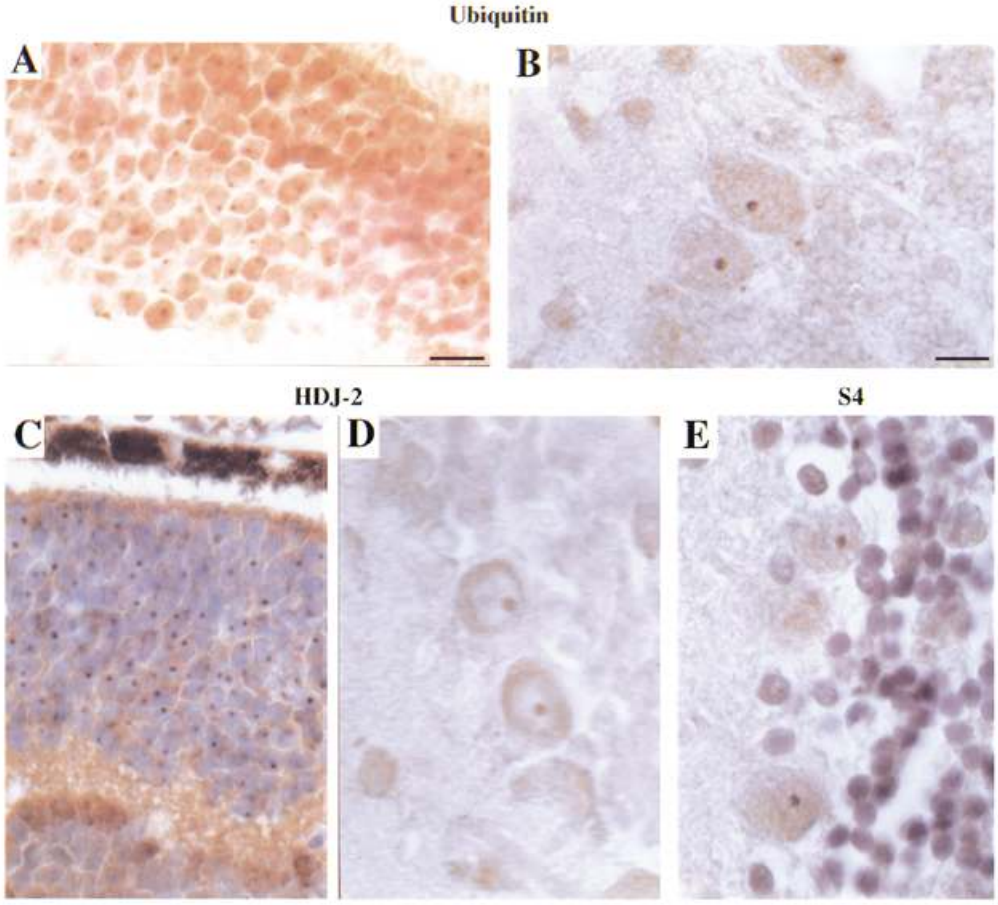

Figure 4. NI immunoreactivity for ubiquitin, chaperone and proteasome subunits. Retinal paraffin sections (**A** and **C**) from a 7-month-old R7E transgenic animal (line A) and cerebellar paraffin sections (**B**, **D** and **E**) from a 19-month-old P7E transgenic animal (line B) were stained by immunoperoxidase and DAB labeling using antibodies against ubiquitin (A and B); HDJ2 chaperone (C and D) and S4 (E) subunit of the 19S proteasome complex. Sections A, C and E were counter-stained with hematoxylin. Bar, 12 μm.

required for protein degradation. Antigens associated with the 11S complex (PA28α and -β) were present in a minority of NIs.

Interestingly, in nodules 9 and 10 of P7E cerebella, where the formation of NIs occurred later with age, many NIs were negative for proteasomal subunits. This suggests that recruitment of these components is a late response. NI immunoreactivities in R7E photoreceptors and P7E Purkinje cells were comparable, suggesting that the cellular reaction is not cell type specific.

Mutant ataxin-7 induces functional anomalies related to the targeted cells

No obvious visible phenotype was noticed in P7E transgenic animals, even up to 1 year of age. To see whether old P7E transgenic animals have normal coordination and locomotion abilities, we tested their performances at 11 months of age on the accelerating rotating rod apparatus (rotarod) for four consecutive days. A strong difference was observed between wild-type animals and their transgenic littermates (Fig. 5A). On the first day itself, the scores of the wild-type animals were significantly higher than those of the P7E transgenics ($P < 0.01$, Student's *t*-test). During the successive days, the difference dramatically increased. P7E transgenics did not show any evidence of improvement, whereas the wild-type littermates greatly increased their scores. Therefore, P7E transgenics have, like SCA1 mice (28), both an impairment to perform the task and an inability to improve their performance.

We examined the functionality of R7E and R7N transgenic retinas by electroretinography (ERG). R7N transgenic animals showed normal ERG but R7E transgenics had a reduced a-wave response compared with their wild-type littermates (Fig. 5B). This anomaly was already detected at 4 weeks (Fig. 5C). The a-wave amplitude dropped to about one third of the normal amplitude at 7 weeks (Fig. 5C). This phenotype did not worsen at later ages but was rather stable with a similar a-wave response at 5–7 months (Fig. 5D). Two independent R7E lines (lines A and F) showed this phenotype (Fig. 5D), whereas no such a-wave reduction was observed in R7N transgenic animals tested at 6 months ($n = 6$ animals; data not shown).

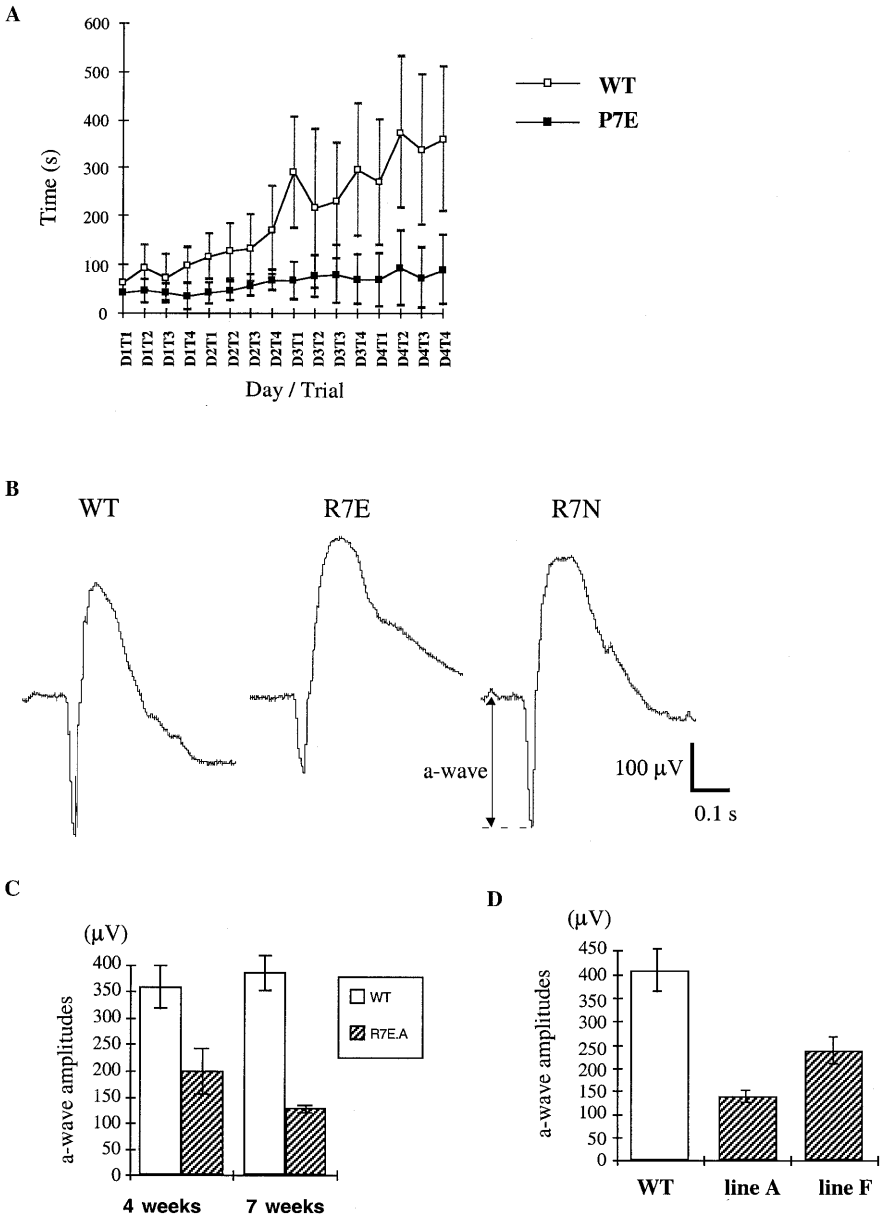

Figure 5. Mutant ataxin-7-mediated dysfunction in transgenic mice. (**A**) Reduced performances of P7EB transgenic animals on the accelerating rod apparatus. Eleven-month-old transgenic (black; $n = 7$) and wild-type (white; $n = 7$) animals were tested in four trials (T) per day for four consecutive days (D) by measuring the time spent on the rod. Bars represent 95% confidence intervals. Repeated-measure ANOVA (see Materials and Methods) demonstrates a genotype effect of $P = 5.05 \times 10^{-4}$ and a day by genotype interaction of $P = 4.2 \times 10^{-5}$. (**B**) Electroretinograms of wild-type, R7E and R7N transgenic animals (age, 5–6 months). (**C**) Reduced a-wave amplitude in young R7E transgenics (4 weeks old; $n = 4$; 7 weeks old; $n = 5$) compared with wild-type littermates (4 weeks old; $n = 3$; 7 weeks old, $n = 3$) in line A. Differences are significant at the level of $P < 0.03$ at 4 weeks old and $P < 0.02$ at 7 weeks old (Wilcoxon tests). Bars, SEM. (**D**) Reduced a-wave amplitude in two distinct R7E lines. Five- to seven-month-old transgenic animals from line R7E.A ($n = 5$), R7E.F ($n = 7$) and age-matched wild-types ($n = 4$) were recorded. Bars, SEM. One-way ANOVA followed by Newman–Keuls comparisons revealed significant effects of the R7E.A ($P < 0.01$) and R7E.F ($P < 0.01$) transgenes compared with wild-type, whereas the difference between the two lines was not significant.

Overexpression of mutant ataxin-7 induces neurodegeneration of the targeted cells

We examined the retinas from wild-type, R7E and R7N transgenic animals by light, electron and immunofluorescence microscopy. Pathological changes were observed in R7E, and not in R7N animals (Fig. 6). No histological anomaly was visible at 2 weeks of age. First signs of pathology were clearly visible at 1 month, a time when NIs are already prominent, the thickness of the outer and inner segment layers was reduced and the outer nuclear layer (ONL) displayed early variations in thickness giving a 'wavy' aspect. A few photoreceptor nuclei were mislocalized in the inner or outer segment layers. At 2.7 months of age, the 'wavy' shape of the ONL was more pronounced, putting some nuclei in contact with the pigment

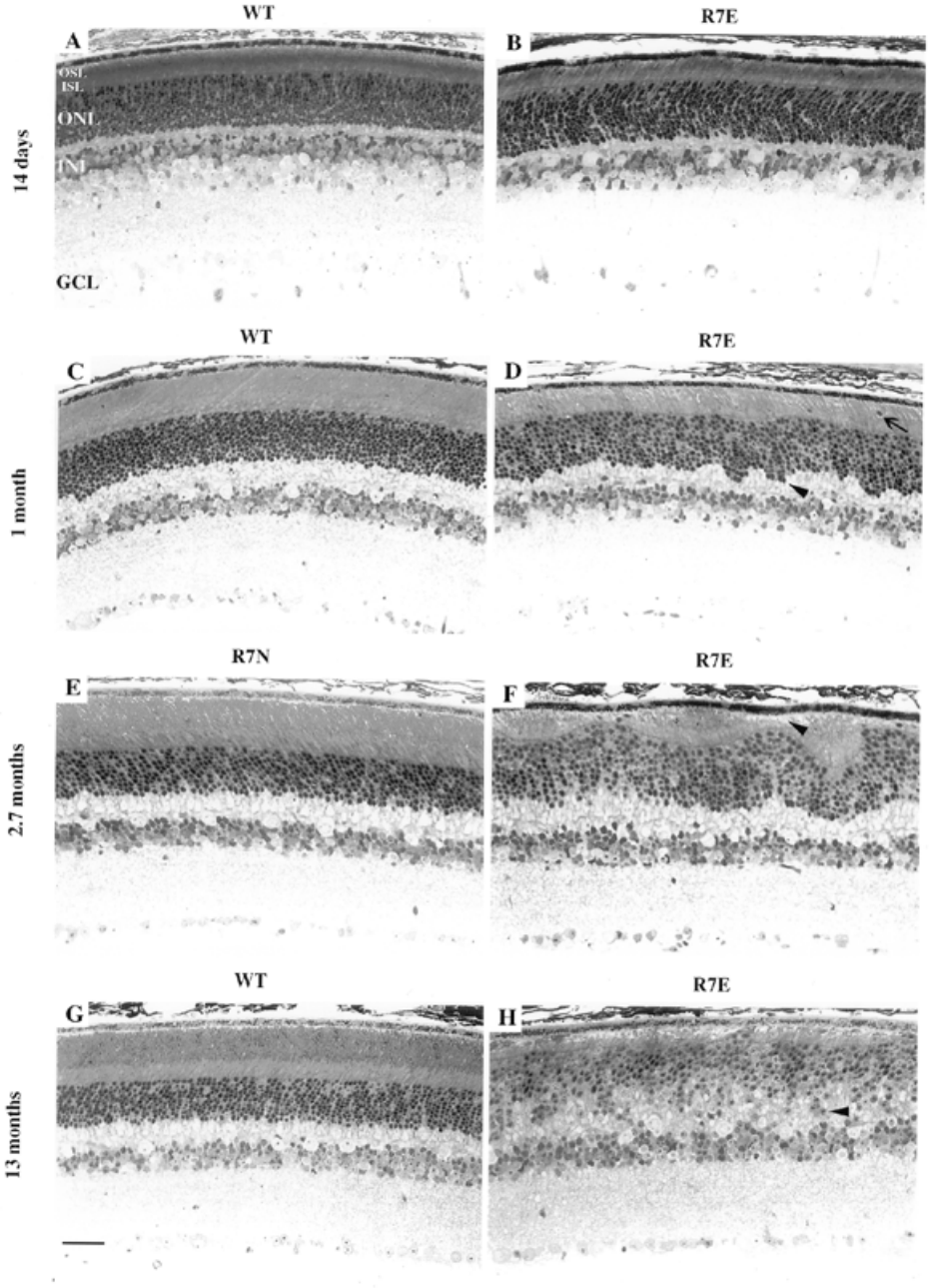

Figure 6. Progressive retinal degeneration in R7E animals. R7E transgenic animals have severe histological anomalies compared with wild-type littermates or age-matched R7N transgenics. Semi-thin sections of retinas from R7E (line A) transgenic and wild-type littermates or from R7N (line C) transgenic animals were stained with Toluidin blue. (**A** and **B**) No anomaly is visible at 14 days of age. (**C** and **D**) At 1 month, the outer nuclear layer of R7E animals starts to present abnormal 'waves' (arrowhead). Some photoreceptor cells are misplaced in the segment layer (arrow). (**E** and **F**) At 2.7 months, the R7E outer nuclear layer is totally disorganized, with some parts already almost adjacent to the pigmental epithelium (arrowhead), whereas R7N transgenic retinas show no abnormality. (**G** and **H**) At 13 months, photoreceptors are still present but with almost no segments. The outer plexiform layer is disorganized, with some photoreceptors flanking the inner nuclear layer (arrowhead). OSL, outer segment layer; ISL, inner segment layer; ONL, outer nuclear layer; INL, inner nuclear layer; GCL, ganglion cell layer. Bar, 60 µm.

epithelium. Segments remained intact in only few parts of the retina. Many photoreceptor nuclei were misplaced into the inner and outer segment layers. At 13 months old, photoreceptors were still present but had lost almost completely their outer segments. Cell nuclei were found in the outer plexiform layer. Numbers of photoreceptor nuclei were reduced by ~30% at 13 months, with regional variations throughout the retina. No obvious cell loss was seen in the inner nuclear layer. Electron microscopy examinations showed that the remaining outer segments were not parallel to one another, were dilated, had lost their parallelism and that their membranous disks were not properly aligned. Membranous debris were frequent in the inner and outer segment layers (Fig. 7A).

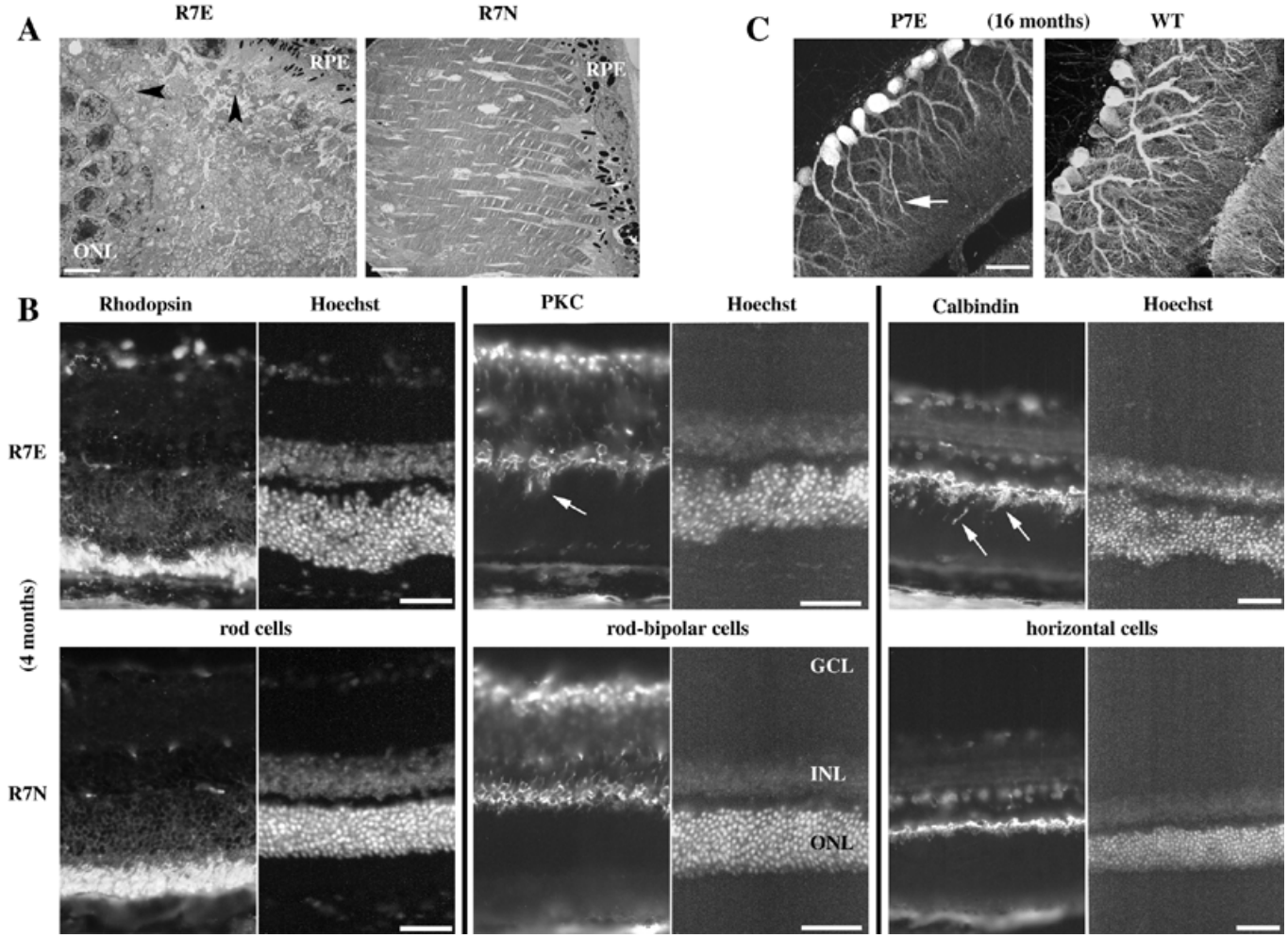

Figure 7. Pathology of ataxin-7[Q90]-expressing cells and their partners. (**A**) Electron microscopy of retinas from 2.7-month-old R7E and R7N transgenic animals. Outer segments are normal in R7N transgenics, whereas the R7E retina shows debris in outer segments (arrowheads) and disorganized inner segments. ONL, outer nuclear layer; RPE, reticulum pigmentary epithelium. Bar, 5 μm. (**B**) Immunofluorescence of 4-month-old R7E and R7N transgenic animals using the rhodopsin, calbindin and PKC markers. No anomaly is found in the R7N animal. The shrunken segments of R7E photoreceptors are labeled with rhodopsin. Horizontal (calbindin-positive) and rod-bipolar (PKC-positive) cells show abnormal neurites infiltrating the outer nuclear layer (arrows). Bar, 60 μm. (C) Calbindin immunofluorescence staining of sections from 16-month-old P7E and wild-type littermates. Purkinje cells of the P7E animal display a reduced dendritic arbor (arrow). Bar, 60 μm.

Staining of rods by immunofluorescence using anti-rhodopsin (Fig. 7B) and anti-arrestin (data not shown) antibodies showed that these proteins are still produced and their distribution paralleled the shrinkage of the outer segments. At 7 months old, R7E, R7N and wild-type retinal sections were stained with an anti-GFAP antibody and we observed immunoreactive Müller cells in all three animals, with focally increased signal in scattered areas of R7E retinas (data not shown). No microglial activation was detected using anti-Mac1 and anti-F4/80 immunomarkers (data not shown).

Examination of cerebellum of P7E animals at 11 months did not show any obvious degenerative phenotype of Purkinje cells nor of the overall anatomy of the cerebellum. At 16 months, however, there was a marked reduction in the dendritic arbour as demonstrated by calbindin immunohistochemistry (Fig. 7C). In addition, there appeared to be a reduction in the density of Purkinje cells, most notably in parasagittal stripes.

Overexpression of mutant ataxin-7 induces trans-neuronal alterations of post-synaptic neurons

Labeling of rod-bipolar cells using an anti-protein kinase C (PKC) antibody (29) showed that these cells displayed morphological anomalies (Fig. 7B). In R7N transgenic animals (as in wild-type; data not shown), fine rod-bipolar cell dendrites in the outer plexiform layer extended into the layer of rod synaptic terminals, whereas R7E retina showed PKC-positive processes infiltrating the ONL. Similar anomalies were found for horizontal cells stained with an anti-calbindin antibody (30) (Fig. 7B). In R7N retina, the processes of horizontal cells ramified normally into the outer plexiform layer but not beyond, whereas in R7E animals, calbindin-positive processes extended within the width of the ONL. The extended processes of both bipolar and horizontal cells were particularly abundant within invaginations due to the 'wavy' aspects of the ONL, some even penetrating the ONL between cell nuclei. The

processes were already detected at 2 months of age and were also immunoreactive for an anti-neurofilament (NF200) antibody (data not shown). Since the transgene was not expressed in all rods, we examined whether these ectopic projections occurred towards or away from areas with dense ataxin-7[Q90] expression. This was done by double-labeling R7E sections with the calbindin or PKC markers and the 1261 antibody. No obvious correlation was observed between the cellular anomalies and the density of ataxin-7[Q90]-positive rods (data not shown).

In cerebellar sections from a 16-month-old P7E animal, stained with an anti-ubiquitin antibody, we observed a marked increase in neuritic immunoreactivity in deep cerebellar nuclei, compatible with either a degeneration of Purkinje cell axonal terminals or alterations of post-synaptic neurites (data not shown).

DISCUSSION

We have generated two mouse models of SCA7, in which expression of full-length ataxin-7 was obtained either in Purkinje cells or in rod photoreceptors, two cell types affected in the human disease. In both models, expression of ataxin-7[Q90] leads to the formation of ubiquitin and proteasome-immunoreactive NIs composed of an N-terminal fragment of the protein. Ataxin-7[Q90] causes dysfunction and signs of degeneration of the targeted cell types, whereas expression of ataxin-7[Q10] induces no such phenotype.

Molecular aspects of mutant ataxin-7 toxicity

Polyglutamine-containing proteins share many common aspects in their pathogenic molecular features, like the formation of aggregates like intranuclear inclusions. However, in respect to their subcellular localization, one can differentiate them in two types. Huntingtin and atrophin-1 normally localize to the cytoplasm and when mutated they partially translocate to the nucleus where they accumulate and aggregate. This translocation is believed to be correlated to a proteolytic cleavage that would generate a truncated fragment of higher toxicity (7,16,17). In contrast, ataxin-1 localizes in both the cytoplasm and the nucleus of Purkinje cells and the pathogenesis of SCA1 is not associated with any proteolytic event. Corresponding NIs are immunoreactive for both extremities of the protein (8).

We show here that ataxin-7 shares common properties with both subgroups. The protein was known to be nuclear in transfected COS cells and patients' lymphoblastoid cell lines (10,11) and both nuclear and cytoplasmic in neurons (12). In transgenic photoreceptors, we show that the localization of the overexpressed protein can even be different with age. For normal ataxin-7, it is nuclear until the third week and then cytoplasmic. For mutant ataxin-7, it is also nuclear until 3 weeks, in part as NIs. Later, and in some cells only, mutant ataxin-7 localizes to the cytoplasm, showing that it is also able to undergo the change of subcellular localization with age. A few aggregates were found in the inner segments at 1 month, indicating that the aggregation process can occur outside the nucleus. These cytoplasmic aggregates were absent at later ages, having possibly been cleared during the normal digestion of outer segments by epithelial cells. The proportion of rod cells with cytoplasmic ataxin-7[Q90] decreased with time, suggesting two possible scenarios: ataxin-7[Q90] may later translocate to the nucleus or the full-length cytoplasmic form is subject to increased degradation or decreased synthesis. Indeed, the C-terminal immunoreactivity of ataxin-7[Q90] fades with age and is absent in old animals, whereas that of ataxin-7[Q10] remains. Mutated ataxin-7 may trigger an acceleration of the protein turn-over or a down-regulation of the transgene expression. Moreover, we showed that the C-terminal part of ataxin-7[Q90] is not present in NIs. Although ataxin-7 has the ability to be nuclear in Purkinje cells (like ataxin-1) and young photoreceptors, it shares the properties of huntingtin in terms of proteolytic processing. This processing appears to happen, at least in part, in the nucleus. Because truncated mutant proteins have been shown *in vitro* and *in vivo* to have a much higher aggregation potential, it is likely that the processing step precedes and accelerates the formation of NIs in these models. However, it cannot be excluded that part or all of this processing may occur after aggregation as a result of ubiquitination and proteasomal action on the inclusions. It will be essential to investigate in human SCA7 tissues whether similar events occur.

NIs of SCA7 transgenic mice are, as in humans (4,5), ubiquitinated and they sequester several proteasomal subunits. SCA7 thus resembles the other polyglutamine disorders where involvement of the ubiquitin/proteasome degradation pathway was reported (27,31–33). Proteasome inhibitors can modulate mutant protein aggregation (9,34,35) and ubiquitin conjugating enzyme deficiency can increase ataxin-1-mediated toxicity (9). The precise role of the proteasome machinery in the toxic process remains to be clarified. Ataxin-7[Q90] may be resistant to complete degradation after its normal turn-over and then aggregate by accumulation. It may also misfold during translation and, as a defective ribosomal product (36), be directly targeted to the proteasome. NIs may themselves be substrates for the proteasome machinery. A recent study using mice with inducible expression of the HD mutation showed that degradation of NIs is possible if no more mutant protein is produced (37). In our SCA7 mice, NIs were also immunoreactive for the HDJ-2 chaperone of the Hsp40 family. This protein was already described in SCA1 (32) and SCA3 (38) inclusions and was shown to be able to decrease (32,33) or increase (34) polyglutamine aggregate formation in cell culture systems. Because a striking suppression of polyglutamine toxicity has recently been obtained by overexpression of either Hsp70 or Hsp40 chaperones in flies (39,40), it is essential now to determine which members of these families are implicated in the mammalian toxic process. Modulation of the intracellular concentration of these protective molecules may be a promising route for therapeutic strategies.

Neurodegeneration in SCA7 mice: alterations of targeted cells and their partners

The Purkinje cell layer is one of the primary sites of degeneration in SCA7 as well as in other autosomal dominant ataxias such as SCA1 (2). Previous studies described a mouse model for SCA1 (dubbed B05) which was generated by targeting expression of ataxin-1[Q82] specifically in Purkinje cells (21). Our P7E model is based on the same transgenic approach, using the same promoter to drive ataxin-7[Q90] expression. The SCA1 and SCA7 models can be compared to some extent.

They both show the progressive formation of NIs containing the mutant protein; these inclusions are ubiquitinated and immunoreactive for chaperones and proteasomal subunits and the locomotion deficiencies observed on the rotarod test are similar (28,32). However, the phenotype observed in P7E animals is less severe and rapid than the one described in the B05 SCA1 mice. In our SCA7 model, no obvious locomotion deficiency or ataxia is visible until 11 months of age, whereas B05 mice present abnormal home cage behavior at 3 months and severe ataxia later (28). This may be attributed to several parameters: (i) the nature of the mutant proteins; (ii) possible different expression levels; and (iii) influence of the genetic background, FVB/N in the case of B05 and C57BL/6 × [C57BL/6 × SJL] here. An example of such a host effect was reported for transgenic mice expressing mutant amyloid precursor protein. The same transgene leading to severe neurodegeneration and lethality in FVB/N but to no such consequence in C57BL/6 × [C57BL/6 × SJL] (41). The reduced dendritic arborization observed in Purkinje cells of our old P7E animals is comparable with the first morphological alterations described in B05 mice. However, we never found ectopic Purkinje cells in the molecular layer as described in the late pathology of B05 animals. Further comparison of the two models in the same background will help to clarify the similarities between the toxic mechanisms induced by two different polyglutamine-containing proteins in a given cell type.

The pathological process is much quicker in R7E photoreceptors than in P7E Purkinje cells. Many NIs, dysfunction and signs of degeneration are visible at one month in the former, whereas inclusions appear after several months and no clear signs of degeneration are visible until 1 year. The differences observed in the two mouse models may be due to the very high expression level driven by the rhodopsin promoter (42). Indeed, immunofluorescence performed under similar conditions suggests a higher expression of mutant ataxin-7 in targeted rods than in targeted Purkinje cells. Alternatively, photoreceptors may be more vulnerable to the mutation. In SCA7, although with some variabilities between kindreds, visual and cerebellar symptoms appear simultaneously in the early stages of disease (43,44). Moreover, histopathologic studies in one patient showed complete loss of the Purkinje cell layer but no retinal degeneration (3). This does not suggest an increased vulnerability of photoreceptors.

The signs of degeneration observed in R7E mice start at 1 month old, at a time when NIs are already numerous and when a significant proportion of rods have lost ataxin-7[Q90] C-terminal immunoreactivity. The manifestations include progressive degeneration of outer segments, misplacement of photoreceptors and a 'wavy' aspect of the ONL. Although disorganized, the thickness of the ONL appears relatively preserved. These observations are somewhat similar to histological anomalies described in retinas from SCA7 patients which include total loss of outer segments apart from abnormal and stubby remaining debris, near-total loss of inner segments and misplacement of cell nuclei in the outer segment and outer plexiform layers (45). In contrast, we did not observe marked reduction of the thickness of the ONL and migration of pigment epithelium as described in patients (3,45). However, it is not surprising that the R7E mouse model is only partially comparable to the human SCA7 retinopathy as, in the latter case, neurons of the inner retina also express the mutation and contain NIs (5).

Reduction of the a-wave amplitude on ERGs reflects photoreceptor dysfunction. The a-wave response did not totally disappear with age. This residual signal may be due to remaining functional rods or to the response of cones. Rod- and cone-specific recordings will be needed to discriminate between these possibilities.

Furthermore, abnormalities can be seen in neurons of the inner retina. Rod-bipolar and horizontal cells are the two types of post-synaptic neuron connected to rod photoreceptors. Although they do not express the transgene in R7E mice they develop abnormal dendritic outgrowth towards and within the ONL. Expression of mutant ataxin-7 in one cell type can therefore induce morphological alterations of downstream neurons. Our observations are very similar to the description of these interneurons in experimental retinal detachment, during which photoreceptors lose their outer segments and eventually die (46). The ectopic processes of horizontal cells in R7E animals are also comparable to the dendritic sprouting of these cells in human retinitis pigmentosa (47). Trans-neuronal responses have long been debated in HD and other polyglutamine disorders (2,48). Does secondary degeneration occur because of the primary cell loss or by the same, cell-autonomous mechanism? Dendritic reorganization was reported in cortical pyramidal neurons of HD (49). Our data suggest now that this plasticity may be a transcellular response to the toxic process induced by mutant huntingtin in partner cells. Such a trans-synaptic effect may be a result of excitotoxicity or neurites may merely grow in order to find new functional partners.

Polyglutamine-induced retinal degeneration offers new opportunities

Photoreceptors are a very specialized neuronal type and we cannot exclude the possibility that the mechanism of toxicity in rods might be specific to these cells. However, we showed that many molecular features of targeted rods are shared by targeted Purkinje cells and appear to be similar to those observed in other mouse models of polyglutamine diseases, or in patients' brains. This validates the use of retina as a model for polyglutamine toxicity. Modeling neurodegeneration in the retina provides several new opportunities for investigations. The retina is a highly organized structure and its cell types are well characterized (50). This allowed us to detect anomalies in cell types that do not express the transgene. ERG offers a direct functional monitoring on living animals. Several animal models of polyglutamine disorders do not present any clearly detectable cell death (15,16,51,52) and when cell death can be seen, it is generally as a late stage of the pathology (28). Dysfunction rather than death seems to be the primary sign of disease and functional monitoring is therefore crucial. ERGs can be assayed repeatedly on the same animal, with no risk of bias from learning like in many locomotion or behavioral tests. However, one limitation is that it acquires the response of the whole retina and may not reflect deficiencies occurring in some cells. This can be overcome by single cell recording on slice preparations after sacrificing the animal (53–55). Single cell recording will also help in evaluating the functional properties of interneurons with abnormal neuritic growth mentioned above. Furthermore, the retina is a suitable source

for adult neuronal primary cell and explant culture (56–58). Transgenic photoreceptors can be studied *in vitro* and any potentially protective agent can be tested prior to *in vivo* investigations.

Finally, injections in the subretinal space allows the testing of the neuroprotective effects of both drugs (59,60) and viral constructs *in vivo*. Several vectors are now reported to be efficient for gene delivery in retinal neurons (61,62) and have successfully been used against photoreceptor degeneration (63–66). We are now testing whether vectors coding for chaperones or neurotrophic factors can protect against the degeneration induced by mutant ataxin-7.

MATERIALS AND METHODS

Generation of transgenic animals

The SV40 intron and poly(A) signal from the pcDNAI/Amp (Invitrogen, Groningen, The Netherlands) vector was cloned in *Eco*RI–*Kpn*I sites of pBluescriptSKII+ (Stratagene, La Jolla, CA). The 3.4 kb SCA7 cDNA from clone D1 (1) was then inserted into *Eco*RI to give the pαaIA intermediate construct. A $(CAG)_{90}$ repeat was amplified by PCR as described (1) from a patient's DNA and cloned into *Aat*II–*Nar*I sites of pαaIA to give the pαbIA construct. A 1.6 kb rhodopsin promoter region was amplified by PCR with *pfu* DNA polymerase (Stratagene) from clone pJHN7 (19) kindly provided by Dr J. Bennett, using primers 5′-GCTCTAGACCTT-CCGCCTGGATGTCCTTC-3′ and 5′-GCTCTAGAATGCTGC-GAAGGCCTGAGC-3′, *Xba*I digested and cloned into the *Spe*I site of pαaIA (resp. pαbIA). A 474 bp *Hin*dIII fragment from pJHN7 (enhancer region) was then added at the *Hin*dIII site of the resulting clones to give the R7N (resp. R7E) constructs. The 850 bp *pcp-2* promoter was amplified by PCR with Vent polymerase (New England Biolabs, Hertfordshire, UK) from clone pDN5Z03 (20) kindly provided by Dr H. Orr, using primers 5′-CGGCTAGCGATCATCTTTCTGGGGCTTAAGCA-3′ and 5′-CGGTCGACCCGATCGCCCTGCACGTGGGTCAG-3′, and cloned into the *Sma*I site of pαaIA (resp. pαbIA) to give the P7N (resp. P7E) constructs.

All final constructs were confirmed by sequencing and the homogeneity of CAG repeats of the final plasmid preparations was checked on Southern blot by probing *Aat*II–*Nar*I digests with a $(CAG)_{10}$ oligoprobe. The final plasmids were *Bss*HII digested to remove bacterial sequences, purified on sucrose gradient and microinjected into [C57BL/6 50%; SJL 50%] fertilized eggs (67). Mouse tail DNA was screened by PCR for the presence of the transgene. The segregation of different integration sites and the approximate copy numbers were assessed by Southern blot using enzymes cutting only once in the transgene (*Pvu*II for P7E and P7N, *Ase*I for R7E and R7N) and a transgene-specific probe covering the SCA7 3′-UTR and SV40 maturation cassette (*Pvu*II fragment of pαaIA construct). The loss of the *rd* allele from the SJL background was checked by PCR and *Dpn*I digest (23).

Western blotting

CHO cells were transfected using calcium phosphate precipitation. Whole cell extracts from CHO cells or LCL were obtained by homogenization in 50 mM Tris–HCl pH 8.0, 10% (v/v) glycerol, 5 mM EDTA, 150 mM KCl, 1 mM PMSF followed by sonication. Retinas were dissected and homogenized in SDS-lysis buffer containing 100 mM Tris–HCl pH 9, 2% SDS, 5% β-mercaptoethanol and 15% glycerol and boiled for 10 min. Total protein extracts were analyzed on 8% SDS–PAGE gel. Primary antibodies were used at 1:2000 for 1C2 (10) and 1:10 000 for γ-tubulin (Sigma, St Louis, MO) and revealed with peroxidase-conjugated secondary antibody (Jackson Laboratories, West Grove, PA) and the ECL chemiluminescent reaction (Pierce, Rockford, IL).

Rotarod

Naive animals were tested for their ability to improve motor skill performance on the rotating rod apparatus (Panlab, Barcelona, Spain). Mice were placed on the rotating rod for four trials per day for four consecutive days. The rod underwent a linear acceleration from 4 to 40 r.p.m. during 10 min. Animals were scored for their latency to fall, which was always <10 min. They were given a resting time of at least 10 min between trials. Results were analyzed by a repeated-measure ANOVA test considering three factors: days (fixed); genotype (fixed); animals (variable), nested in genotype and crossed with days.

Electroretinography

Dark-adapted animals were anesthetized with an intraperitoneal injection (23 µl/g) of etomidate (0.2 mg/ml) and midazolan (1.25 mg/ml). Pupils were dilated with 0.5% tropicamide application and the cornea was locally anesthetized with 0.5% topical proparacaine application. Upper and lower lids were retracted to proptose and maintain the eye open. A stainless steel reference electrode was inserted subcutaneously on the head of the animal. ERGs were then measured with a saline-soaked cotton wick placed at the apex of the cornea and connected to an Ag:AgCl electrode. Responses were amplified and filtered [0.1 Hz (low) and 1000 Hz (high) cut-off filters] with a Universal amplifier (Gould, TX). They were digitized using a data acquisition labmaster board (Scientific Solutions, Solon, OH) mounted on an IBM-compatible personal computer. A 150 watt xenon lamp bulb (Müller Instruments, Moosinning, Germany) provided the light stimulus of 2.9 log cd/m^2 as measured with a luxmeter at eye level. The duration of the light stimulus (300 ms) was defined by a computer-controlled shutter.

Antibodies

The antibodies, 1597 and 1598, were obtained by injecting rabbits with peptide N-CTIPGAQGLMNSSLLHQPKAR-C coupled to ovalbumin. Sera were affinity-purified against the antigen peptide using a Sulfolink column (Pierce) and stored in 1% ovalbumin. Their specificity was assessed on a western blot of COS cells transfected with SCA7 cDNA. The 1598 (as well as 1261) did not lead to any signal when used with immunofluorescence on non-trangenic mouse retinas. The 1261 and 1C1 antibodies were obtained as described by Lindenberg *et al.* (12). Table 3 lists the source of the antibodies used and the working dilutions.

Table 3. The source of the antibodies used and the working dilutions

Antibodies	Dilution for IF	Dilution for IHC	Source
1598	1:1000	1:2000	Authors
1261	1:100	1:100	Authors
1C1	1:100	1:400	Authors
HDJ-1/Hsp40	ND	1:500	MBL (Japan)
HDJ-2/Hsp40	ND	1:500	Neomarkers
Ubiquitin	ND	1:10 000	Biotrend
11Sα	ND	1:1000	Affiniti
11Sβ	ND	1:1000	Affiniti
19S_S4	ND	1:500	Affiniti
19S_S5a	ND	1:250	Affiniti
19S_S6b	ND	1:1000	Affiniti
19S_S7	ND	1:2000	Affiniti
19S_S10b	ND	1:500	Affiniti
20S_α3	ND	1:500	Affiniti
20S_αall	ND	1:2000	Affiniti
20S_β2	ND	1:500	Affiniti
20S_β3	N.D	1:200	Affiniti
Calbindin	1:10 000	ND	Sigma
PKC (MC5)	1:200	ND	Sigma
Rho4D2	1:1000	ND	Gift from D.Hicks

ND, not determined.

Tissue fixation

Retinas. For immunohistochemistry and immunofluorescence, enucleated eyes were dissected to remove lens and cornea and fixed by immersion in 4% paraformaldehyde for 1 h, 0.3 mM $CaCl_2$, 0.1 mM $MgCl_2$, 1× PBS. For light and electron microscopy, eyes were fixed by immersion in 2.5% glutaraldehyde in 0.1 M cacodylate buffer pH 7.4, for 16 h at 4°C and the lenses removed.

Cerebelli. Animals were anesthetized by intraperitoneal injection of a sublethal dose of 100 mg/ml ketamin, 5 mg/ml chlorobutanol, 8 mg/ml xylazin base, 0.4 mg/ml methylparabenzoate (Imalgene1000; Merial and Rompun, Lyon, France) in 0.9% saline solution and intracardially perfused with 10 ml of 0.9% saline solution followed by 100 ml of 4% paraformaldehyde, 1× PBS. Brains were then dissected and post-fixed by immersion (same fixative) for 1 h.

Immunohistochemistry

Fixed tissues were embedded in paraffin and cut into 5 µm sections which were stained as follows: after deparaffination, slides were rehydrated in a graded series of ethanol (100% × 2, 95% × 2, 80%, 70%; for 5 min each), boiled in 10 mM citrate buffer (pH 6.0) in a microwave, washed in 1× PBS, blocked of the endogenous peroxidase with methanol/H_2O_2 (40:1% in H_2O) for 10 min, washed in 1× PBS, blocked for 30 min [1× PBS + 0.3% Triton X-100, 5% normal goat serum (primary polyclonal rabbit antibody) or 5% normal horse serum (primary monoclonal mouse antibody)]. Sections were then rinsed in 1× PBS followed by incubation in a humid chamber at 4°C with the primary antibody for 36 h. Secondary antibodies [Vector biotinylated anti-mouse IgG (H+L), biotinylated anti-rabbit IgG (H+L), respectively] (diluted 1:200) were applied for 30 min at room temperature and visualized using the avidin–biotin–peroxidase complex method (Vectastain elite kit; Vector Laboratories, Burlingame, CA). The color reaction was carried out using FAST DAB tablets (Sigma). Some sections were lightly counterstained with hematoxylin, sections were dehydrated through graded ethanols and xylene and viewed using a light microscope.

Immunofluorescence

Fixed retinas were placed for 30 min in 30% sucrose, 1× PBS and frozen in OCT medium. Cryostat sections (9 µm) were mounted on gelatinized slides, permeabilized for 5 min with 0.1% Triton X-100, 1× PBS, blocked for 15 min with 0.5% bovine serum albumin, 0.1% Tween-20, 1× PBS. Primary and secondary antibodies (Cy3, FITC or Oregon Green conjugated; Jackson ImmunoResearch Laboratories) were diluted in this blocking solution for 2 h incubations.

Fixed brains were incubated overnight in 30% sucrose, 1× PBS and snap-frozen on dry ice. Fifty micrometer free-floating sections were blocked in 5% goat serum, 0.3% Triton X-100, 1× PBS, washed in PBS and incubated with primary and secondary antibodies (same as above) diluted in 5% goat serum, 1× PBS.

Light and electron microscopy

Fixed eyes were rinsed in cacodylate buffer, postfixed in 1% osmium tetroxide in the same buffer for 2 h at 4°C, dehydrated with graded alcohol series and embedded in Epon. Sections (1 µm) were stained with toluidin blue. Cell nuclei were counted on retinal sections, in a 150 µm window situated at a distance of 200 µm from the optic nerve. For electron microscopy, ultrathin sections from selected areas were contrasted with uranyl acetate and lead citrate and examined with a Philips 208 electron microscope operating at 80 kV. For the visualization of inclusions, retinas were isolated, fixed in 4% paraformaldehyde, 0.3 mM $CaCl_2$, 0.1 mM $MgCl_2$, 1× PBS for 1 h at 4°C, cut into floating pieces, rinsed in PBS, treated for 10 min in 40% methanol, 1% H_2O_2, rinsed in PBS, permeabilized for 8 min in 0.1% Triton, PBS, rinsed, blocked in 0.5% bovine serum albumin, 0.1% Tween-20, 1× PBS, incubated for 2 h with the 1261 antibody (1:100 dilution), rinsed and revealed with the same peroxidase and DAB kit as for immunohistochemistry (see above). Pieces of retina were finally incubated in 2.5% glutaraldehyde and proceeded as for the eyes.

ACKNOWLEDGEMENTS

We thank D. Devys, Y. Trottier, D. Hicks, A. Lunkes, T. Leveillard and D. Helmlinger for fruitful discussions; M. Le Meur and staff at the IGBMC animal facility for microinjections and mouse care; J. Bennett for advice and gift of the

rhodopsin promoter; H. Orr for the *pcp-2* promoter; C. Weber, V. Forster, E. Simonutti and M. Gendron for priceless technical assistance; P. Eberling and G. Duval for help in generating the 1598 and 1597 antibodies; A. Ganzmüller for light and electron microscopy; J.-L. Vonesh, D. Hentsch and R. Knoth for confocal imaging; A.-S. Lebre for a clone containing the $(CAG)_{90}$ expansion; and the cell line library of INSERM U289 for the SCA7 patient cell line. This work was supported by funds from the Institut National de la Santé et de la Recherche Médicale, the Centre National de la Recherche Scientifique, the Hôpital Universitaire de Strasbourg, Fondation Louis Jeantet and by a grant of the DFG (SFB 505, TP C2) to K.S.L. and G.B.L. G.Y. was supported by a fellowship from the Fondation pour la Recherche Medicale.

REFERENCES

1. David, G., Abbas, N., Stevanin, G., Durr, A., Yvert, G., Cancel, G., Weber, C. *et al*. (1997) Cloning of the SCA7 gene reveals a highly unstable CAG repeat expansion. *Nature Genet.*, **17**, 65–70.
2. Wells, R.D. and Warren, S.T. (1998) *Genetic Instabilities and Hereditary Neurological Diseases.* Academic Press, San Diego, CA.
3. Martin, J.J., Van Regemorter, N., Krols, L., Brucher, J.M., de Barsy, T., Szliwowski, H., Evrard, P. *et al.* (1994) On an autosomal dominant form of retinal-cerebellar degeneration: an autopsy study of five patients in one family. *Acta Neuropathologica*, **88**, 277–286.
4. Holmberg, M., Duyckaerts, C., Dürr, A., Cancel, G., Gourfinkel-An, I., Damier, P., Faucheux, B. *et al.* (1998) Spinocerebellar ataxia type 7 (SCA7): a neurodegenerative disorder with neuronal intranuclear inclusions. *Hum. Mol. Genet.*, **7**, 913–918.
5. Mauger, C., Del-Favero, J., Ceuterick, C., Lubke, U., van Broeckhoven, C. and Martin, J. (1999) Identification and localization of ataxin-7 in brain and retina of a patient with cerebellar ataxia type II using anti-peptide antibody. *Mol. Brain Res.*, **74**, 35–43.
6. Di Figlia, M., Sapp, E., Chase, K.O., Davies, S.W., Bates, G.P., Vonsattel, J.P. and Aronin, N. (1997) Aggregation of Huntingtin in neuronal intranuclear inclusions and dystrophic neurites in brain. *Science*, **277**, 1990–1993.
7. Gutekunst, C.A., Li, S.H., Yi, H., Mulroy, J.S., Kuemmerle, S., Jones, R., Rye, D. *et al.* (1999) Nuclear and neuropil aggregates in Huntington's disease: relationship to neuropathology. *J. Neurosci.*, **19**, 2522–2534.
8. Klement, I.A., Skinner, P.J., Kaytor, M.D., Yi, H., Hersch, S.M., Clark, H.B., Zoghbi, H.Y. *et al.* (1998) Ataxin-1 nuclear localization and aggregation: role in polyglutamine-induced disease in SCA1 transgenic mice. *Cell*, **95**, 41–53.
9. Cummings, C.J., Reinstein, E., Sun, Y., Antalffy, B., Jiang, Y., Ciechanover, A., Orr, H.T. *et al.* (1999) Mutation of the E6-AP ubiquitin ligase reduces nuclear inclusion frequency while accelerating polyglutamine-induced pathology in SCA1 mice. *Neuron*, **24**, 879–892.
10. Trottier, Y., Lutz, Y., Stevanin, G., Imbert, G., Devys, D., Cancel, G., Saudou, F. *et al.* (1995) Polyglutamine expansion as a pathological epitope in Huntington's disease and four dominant cerebellar ataxias. *Nature*, **378**, 403–406.
11. Kaytor, M.D., Duvick, L.A., Skinner, P.J., Koob, M.D., Ranum, L.P. and Orr, H.T. (1999) Nuclear localization of the spinocerebellar ataxia type 7 protein, ataxin-7. *Hum. Mol. Genet.*, **8**, 1657–1664.
12. Lindenberg, K., Yvert, G., Müller, K. and Landwehrmeyer, B. (2000) Expression of ataxin-7 mRNA and protein in human brain: evidence for a widespread distribution and focal protein accumulation. *Brain Pathol.*, **10**, 385–394.
13. Davies, S.W., Turmaine, M., Cozens, B.A., Difiglia, M., Sharp, A.H., Ross, C.A., Scherzinger, E. *et al.* (1997) Formation of neuronal intranuclear inclusions underlies the neurological dysfunction in mice transgenic for the HD mutation. *Cell*, **90**, 537–548.
14. Reddy, P.H., Williams, M., Charles, V., Garrett, L., Pike-Buchanan, L., Whetsell, W.O., Miller, G. *et al.* (1998) Behavioral abnormalities and selective neuronal loss in HD transgenic mice expressing mutated full length HD cDNA. *Nature Genet.*, **20**, 198–202.
15. Schilling, G., Becher, M.W., Sharp, A.H., Jinnah, H.A., Duan, K., Kotzuk, J.A., Slunt H.H. *et al.* (1999) Intranuclear inclusions and neuritic aggregates in transgenic mice expressing a mutant N-terminal fragment of huntingtin. *Hum. Mol. Genet.*, **8**, 397–407.
16. Schilling, G., Wood, J.D., Duan, K., Slunt, H.H., Gonzales, V., Yamada, M., Cooper, J.K. *et al.* (1999) Nuclear accumulation of truncated atrophin-1 fragments in a transgenic mouse model of DRPLA. *Neuron*, **24**, 275–286.
17. Wheeler, V.C., White, J.K., Gutekunst, C.A., Vrbanac, V., Weaver, M., Li, X.J., Li, S.H. *et al.* (2000) Long glutamine tracts cause nuclear localization of a novel form of huntingtin in medium spiny striatal neurons in HdhQ92 and HdhQ111 knock-in mice. *Hum. Mol. Genet.*, **9**, 503–513.
18. Bennett, J., Sun, D. and Kariko, K. (1995) Sequence analysis of the 5.34 kb 5′ flanking region of the human rhodopsin-encoding gene. *Gene*, **167**, 317–320.
19. Nathans, J. and Hogness, D.S. (1984) Isolation and nucleotide sequence of the gene encoding human rhodopsin. *Proc. Natl Acad. Sci. USA*, **81**, 4851–4855.
20. Vandaele, S., Nordquist, D.T., Feddersen, R.M., Tretjakoff, I., Peterson, A.C. and Orr, H.T. (1991) Purkinje cell protein-2 regulatory regions and transgene expression in cerebellar compartments. *Gene Dev.*, **5**, 1136–1148.
21. Burright, E.N., Clark, H.B., Servadio, A., Matilla, T., Feddersen, R.M., Yunis, W.S., Duvick, L.A. *et al.* (1995) SCA1 transgenic mice: a model for neurodegeneration caused by an expanded CAG trinucleotide repeat. *Cell*, **82**, 937–948.
22. Nie, Z., Chen, S., Kumar, R. and Zack, D.J. (1996) RER, an evolutionarily conserved sequence upstream of the rhodopsin gene, has enhancer activity. *J. Biol. Chem.*, **271**, 2667–2675.
23. Pittler, S.J. and Baehr, W. (1991) Identification of a nonsense mutation in the rod photoreceptor cGMP phosphodiesterase beta-subunit gene of the rd mouse. *Proc. Natl Acad. Sci. USA*, **88**, 8322–8326.
24. Strait, K.A., Zou, L. and Oppenheimer, J.H. (1992) Beta 1 isoform-specific regulation of a triiodothyronine-induced gene during cerebellar development. *Mol. Endocrin.*, **6**, 1874–1880.
25. Del-Favero, J., Krols, L., Michalik, A., Theuns, J., Lofgren, A., Goossens, D., Wehnert, A. *et al.* (1998) Molecular genetic analysis of autosomal dominant cerebellar ataxia with retinal degeneration (ADCA type II) caused by CAG triplet repeat expansion. *Hum. Mol. Genet.*, **7**, 177–186.
26. Michalik, A., Del-Favero, J., Mauger, C., Lofgren, A. and Van Broeckhoven, C. (1999) Genomic organisation of the spinocerebellar ataxia type 7 (SCA7) gene responsible for autosomal dominant cerebellar ataxia with retinal degeneration. *Hum. Genet.*, **105**, 410–417.
27. Ferrigno, P. and Silver, P.A. (2000) Polyglutamine expansions: proteolysis, chaperones, and the dangers of promiscuity. *Neuron*, **26**, 9–12.
28. Clark, H.B., Burright, E.N., Yunis, W.S., Larson, S., Wilcox, C., Hartman, B., Matilla, A. *et al.* (1997) Purkinje cell expression of a mutant allele of SCA1 in transgenic mice leads to disparate effects on motor behaviors followed by a progressive cerebellar dysfunction and histological alterations. *J. Neurosci.*, **17**, 7385–7395.
29. Greferath, U., Grunert, U. and Wassle, H. (1990) Rod bipolar cells in the mammalian retina show protein kinase C-like immunoreactivity. *J. Comp. Neurol.*, **301**, 433–442.
30. Johnson, J., Wu, V., Wong, H., Walsh, J.H. and Brecha, N.C. (1999) Somatostatin receptor subtype 2A expression in the rat retina. *Neuroscience*, **94**, 675–683.
31. Chai, Y., Koppenhafer, S.L., Shoesmith, S.J., Perez, M.K. and Paulson, H.L. (1999) Evidence for proteasome involvement in polyglutamine disease: localization to nuclear inclusions in SCA3/MJD and suppression of polyglutamine aggregation *in vitro*. *Hum. Mol. Genet.*, **8**, 673–682.
32. Cummings, C.J., Mancini, M.A., Antalffy, B., DeFranco, D.B., Orr, H.T. and Zoghbi, H.Y. (1998) Chaperone suppression of aggregation and altered subcellular proteasome localization imply protein misfolding in SCA1. *Nature Genet.*, **19**, 148–154.
33. Stenoien, D.L., Cummings, C.J., Adams, H.P., Mancini, M.G., Patel, K., DeMartino, G.N., Marcelli, M. *et al.* (1999) Polyglutamine-expanded androgen receptors form aggregates that sequester heat shock proteins, proteasome components and SRC-1, and are suppressed by the HDJ-2 chaperone. *Hum. Mol. Genet.*, **8**, 731–741.
34. Wyttenbach, A., Carmichael, J., Swartz, J., Furlong, R.A., Narain, Y., Rankin, J. and Rubinsztein, D.C. (2000) Effects of heat shock, heat shock protein 40 (HDJ-2), and proteasome inhibition on protein aggregation in cellular models of Huntington's disease. *Proc. Natl Acad. Sci. USA*, **97**, 2898–2903.
35. de Cristofaro, T., Affaitati, A., Cariello, L., Avvedimento, E.V. and Varrone, S. (1999) The length of polyglutamine tract, its level of expres-

sion, the rate of degradation, and the transglutaminase activity influence the formation of intracellular aggregates. *Biochem. Biophys. Res. Commun.*, **260**, 150–158.
36. Schubert, U., Anton, L.C., Gibbs, J., Norbury, C.C., Yewdell, J.W. and Bennink, J.R. (2000) Rapid degradation of a large fraction of newly synthesized proteins by proteasomes. *Nature*, **404**, 770–774.
37. Yamamoto, A., Lucas, J.J. and Hen, R. (2000) Reversal of neuropathology and motor dysfunction in a conditional model of Huntington's disease. *Cell*, **101**, 57–66.
38. Chai, Y., Koppenhafer, S.L., Bonini, N.M. and Paulson, H.L. (1999) Analysis of the role of heat shock protein (Hsp) molecular chaperones in polyglutamine disease. *J. Neurosci.*, **19**, 10338–10347.
39. Kazemi-Esfarjani, P. and Benzer, S. (2000) Genetic suppression of polyglutamine toxicity in *Drosophila*. *Science*, **287**, 1837–1840.
40. Warrick, J.M., Chan, H.Y.E., Gray-Board, G.L., Chai, Y., Paulson, H.L. and Bonini, N.M. (1999) Suppression of polyglutamine-mediated neurodegeneration in Drosophila by the molecular chaperone Hsp70. *Nature Genet.*, **23**, 425–428.
41. Hsiao, K.K., Borchelt, D.R., Olson, K., Johannsdottir, R., Kitt, C., Yunis, W., Xu, S. *et al.* (1995) Age-related CNS disorder and early death in transgenic FVB/N mice overexpressing Alzheimer amyloid precursor proteins. *Neuron*, **15**, 1203–1218.
42. Olsson, J.E., Gordon, J.W., Pawlyk, B.S., Roof, D., Hayes, A., Molday, R.S., Mukai, S. *et al.* (1992) Transgenic mice with a rhodopsin mutation (Pro23His): a mouse model of autosomal dominant retinitis pigmentosa. *Neuron*, **9**, 815–830.
43. Gouw, L.G., Digre, K.B., Harris, C.P., Haines, J.H. and Ptacek, L.J. (1994) Autosomal dominant cerebellar ataxia with retinal degeneration: clinical, neuropathologic, and genetic analysis of a large kindred. *Neurology*, **44**, 1441–1447.
44. Enevoldson, T.P., Sanders, M.D. and Harding, A.E. (1994) Autosomal dominant cerebellar ataxia with pigmentary macular dystrophy. A clinical and genetic study of eight families. *Brain*, **117**, 445–460.
45. Ryan Jr, S.J., Knox, D.L., Green, W.R. and Konigsmark, B.W. (1975) Olivopontocerebellar degeneration. Clinicopathologic correlation of the associated retinopathy. *Arch. Ophthalmol.*, **93**, 169–172.
46. Lewis, G.P., Linberg, K.A. and Fisher, S.K. (1998) Neurite outgrowth from bipolar and horizontal cells after experimental retinal detachment. *Invest. Ophthalmol. Vis. Sci.*, **39**, 424–434.
47. Fariss, R.N., Li, Z.Y. and Milam, A.H. (2000) Abnormalities in rod photoreceptors, amacrine cells, and horizontal cells in human retinas with retinitis pigmentosa. *Am. J. Ophthalmol.*, **129**, 215–223.
48. Sharp, A.H. and Ross, C.A. (1996) Neurobiology of Huntington's disease. *Neurobiol. Dis.*, **3**, 3–15.
49. Sotrel, A., Williams, R.S., Kaufmann, W.E. and Myers, R.H. (1993) Evidence for neuronal degeneration and dendritic plasticity in cortical pyramidal neurons of Huntington's disease: a quantitative Golgi study. *Neurology*, **43**, 2088–2096.
50. Jeon, C.J., Strettoi, E. and Masland, R.H. (1998) The major cell populations of the mouse retina. *J. Neurosci.*, **18**, 8936–8946.
51. Mangiarini, L., Sathasivam, K., Seller, M., Cozens, B., Harper, A., Hetherington, C., Lawton, M. *et al.* (1996) Exon 1 of the *HD* gene with an expanded CAG repeat is sufficient to cause a progressive neurological phenotype in transgenic mice. *Cell*, **87**, 493–506.
52. Ordway, J.M., Tallaksen-Greene, S., Gutekunst, C.A., Bernstein, E.M., Cearley, J.A., Wiener, H.W., Dure, L.S. *et al.* (1997) Ectopically expressed CAG repeats cause intranuclear inclusions and a progressive late onset neurological phenotype in the mouse. *Cell*, **91**, 753–763.
53. de la Villa, P., Vaquero, C.F. and Kaneko, A. (1998) Two types of calcium currents of the mouse bipolar cells recorded in the retinal slice preparation. *Eur. J. Neurosci.*, **10**, 317–323.
54. Berntson, A. and Taylor, W.R. (2000) Response characteristics and receptive field widths of on-bipolar cells in the mouse retina. *J. Physiol.*, **524**, 879–889.
55. Satoh, H., Aoki, K., Watanabe, S.I. and Kaneko, A. (1998) L-type calcium channels in the axon terminal of mouse bipolar cells. *Neuroreport*, **9**, 2161–2165.
56. Streichert, L.C., Birnbach, C.D. and Reh, T.A. (1999) A diffusible factor from normal retinal cells promotes rod photoreceptor survival in an in vitro model of retinitis pigmentosa. *J. Neurobiol.*, **39**, 475–490.
57. Mohand-Said, S., Deudon-Combe, A., Hicks, D., Simonutti, M., Forster, V., Fintz, A.C., Leveillard, T. *et al.* (1998) Normal retina releases a diffusible factor stimulating cone survival in the retinal degeneration mouse. *Proc. Natl Acad. Sci. USA*, **95**, 8357–8362.
58. Gaudin, C., Forster, V., Sahel, J., Dreyfus, H. and Hicks, D. (1996) Survival and regeneration of adult human and other mammalian photoreceptors in culture. *Invest. Ophthalmol. Vis. Sci.*, **37**, 2258–2268.
59. Frasson, M., Sahel, J.A., Fabre, M., Simonutti, M., Dreyfus, H. and Picaud, S. (1999) Retinitis pigmentosa: rod photoreceptor rescue by a calcium-channel blocker in the rd mouse. *Nature Med.*, **5**, 1183–1187.
60. LaVail, M.M., Yasumura, D., Matthes, M.T., Lau-Villacorta, C., Unoki, K., Sung, C.H. and Steinberg, R.H. (1998) Protection of mouse photoreceptors by survival factors in retinal degenerations. *Invest. Ophthalmol. Vis. Sci.*, **39**, 592–602.
61. Ali, R.R., Reichel, M.B., Thrasher, A.J., Levinsky, R.J., Kinnon, C., Kanuga, N., Hunt, D.M. *et al.* (1996) Gene transfer into the mouse retina mediated by an adeno-associated viral vector. *Hum. Mol. Genet.*, **5**, 591–594.
62. Miyoshi, H., Takahashi, M., Gage, F.H. and Verma, I.M. (1997) Stable and efficient gene transfer into the retina using an HIV-based lentiviral vector. *Proc. Natl Acad. Sci. USA*, **94**, 10319–10323.
63. Lewin, A.S., Drenser, K.A., Hauswirth, W.W., Nishikawa, S., Yasumura, D., Flannery, J.G. and LaVail, M.M. (1998) Ribozyme rescue of photoreceptor cells in a transgenic rat model of autosomal dominant retinitis pigmentosa. *Nature Med.*, **4**, 967–971.
64. Bennett, J., Zeng, Y., Bajwa, R., Klatt, L., Li, Y. and Maguire, A.M. (1998) Adenovirus-mediated delivery of rhodopsin-promoted bcl-2 results in a delay in photoreceptor cell death in the rd/rd mouse. *Gene Ther.*, **5**, 1156–1164.
65. Takahashi, M., Miyoshi, H., Verma, I.M. and Gage, F.H. (1999) Rescue from photoreceptor degeneration in the rd mouse by human immunodeficiency virus vector-mediated gene transfer. *J. Virol.*, **73**, 7812–7816.
66. Cayouette, M. and Gravel, C. (1997) Adenovirus-mediated gene transfer of ciliary neurotrophic factor can prevent photoreceptor degeneration in the retinal degeneration (rd) mouse. *Hum. Gene Ther.* **8**, 423–430.
67. Hogan, B., Costantini, F. and Lacy, E. (1986) *Manipulating the Mouse Embryo: A Laboratory Manual*. Cold Spring Harbor Laboratory Press, Cold Spring Harbor, NY.